Morphology And Degradation Properties Of Pcl/Hyaff11 Composite Scaffolds With Multiscale Degradation Rate

V. Guarino, M. Lewandowska, M. Bil, B. Polak, L. Ambrosio

Morphology And Degradation Properties Of Pcl/Hyaff11 ® Composite Scaffolds With Multiscale Degradation Rate

V. Guarino, M. Lewandowska, M. Bil, B. Polak, L. Ambrosio

PII: S0266-3538(10)00241-1
DOI: 10.1016/j.compscitech.2010.06.015
Reference: CSTE 4750

To appear in: *Composites Science and Technology*

Received Date: 30 November 2009
Revised Date: 10 June 2010
Accepted Date: 20 June 2010

Please cite this article as: Guarino, V., Lewandowska, M., Bil, M., Polak, B., Ambrosio, L., Morphology And Degradation Properties Of Pcl/Hyaff11 ® Composite Scaffolds With Multiscale Degradation Rate, *Composites Science and Technology* (2010), doi: 10.1016/j.compscitech.2010.06.015

MORPHOLOGY AND DEGRADATION PROPERTIES OF PCL/HYAFF11® COMPOSITE SCAFFOLDS WITH MULTISCALE DEGRADATION RATE

V. Guarino[1]*, M. Lewandowska[2]*, M. Bil[2], B. Polak[3], L. Ambrosio[1]

[1] Institute of Composite and Biomedical Materials, CNR Naples, Italy.

[2] Warsaw University of Technology, Faculty of Materials Science and Engineering

[3] Warsaw University of Technology, Faculty of Chemistry

Abstract

The analysis of scaffold degradation is a promising strategy for understanding the dynamic changes in texture and pore morphology which accompany polymer resorption, and for collecting same fundamental indicators regarding the potential fate of the scaffold in the biological environment. In this study, we investigate the morphology and degradation properties of three composite scaffolds based on poly(ε-caprolactone) (PCL) embedded with benzyl ester of hyaluronic acid (HYAFF11®) phases, and, in turn, different reinforcement systems - i.e, calcium phosphate particles or continuous poly(lactic acid) (PLA) fibres. Scanning electron microscopy (SEM) and μ-tomography supported by digital image analysis enabled a not invasive investigation of the scaffold morphology, providing a quantitative assessment of porosity (which ranged from 63.1 to 82.8), pore sizes (which varied from 170.5 to 230.4 μm) and pore interconnectivity. Thermal analyses (DSC and TGA) and Raman spectroscopy demonstrated the multi-scale degradation of the composite with highly tailoring degradation kinetics depending on the component material phases and scaffold architecture changes, due to their conditioning in simulated *in vivo* environment (i.e, SBF solution). These results demonstrate that the judicious mixing of materials with faster (i.e, Hyaff11) and slower (i.e, PLA and PCL) degradation kinetics, different size and shape (i.e, domains, particles or long fibres), certainly concurs to design a smart

composite scaffold with time-controlled degradation which can support the regeneration of a large variety of tissues, from the cartilage to the bone.

Introduction

The architecture and the structural organization of scaffolds are critical factors to assure the functionality of tissue engineered constructs and their appropriate and effective application in health care. It is commonly recognized that porosity actively influences the biological behavior of seeded cells during *in vitro* culture, through the provision of an adequate surface area for cell attachment, stimulating the free circulation of biological fluids and oxygen transport for their maintenance and, subsequently, influencing the *in vivo* conductive response of the structure after its implantation [1][2][3]. In this context, the synchronization of polymer degradation with its replacement by natural tissue produced from cells would be desirable. As a consequence, the degradation properties of a scaffold are relevant both to the biomaterial design and to the long-term success of a tissue engineered construct [4].

To date, much effort has been dedicated to the design of a variety of composite materials for tissue engineering scaffolds with tailored degradation properties, based on biocompatible and bioerodible polymers [5][6]. Recently, several authors have focused their attention on polyester-based composite systems. [7][8][9] The influence of several factors on degradation kinetics are considered [10], including *molecular factors* (e.g., chain orientation, molecular weight, M_w, and polydispersity) *supramolecular factors* (crystallinity, the spatial distribution of chemically reactive filler [11]) and *environmental factors* (e.g., mechanical stimuli). The various influences of these factors potentially generates a wide range of resorbable properties for custom-made systems. However, the evolution of structural properties in connection with the selective degradation of one of the components of the scaffold matrix has not been adequately

explored, despite its significant contribution to the activation and the requisite enabling and support of specific biological mechanisms on an appropriate time-scale.

In the current work, polymeric composite scaffolds based on poly(ε-caprolactone) (PCL) and esters of hyaluronic acid have been proposed because of the encouraging pre-clinical results which similar systems have exhibited as *in vivo* scaffolds for tissue regeneration [12][13]. PCL shows a remarkably slow degradation rate – from 6 months up to 3 years for its complete removal from the host body - as a function of the starting molecular weight [14][15]. Firstly, this preserves mechanical integrity over the degradation lifetime of the device, so allowing adequate mechanical support during the post-implantation period. Secondly, the absence of toxic response, due to the reduced release of acidic products, assures enhanced bone ingrowth into the porous scaffolds supported by the progressive increase of pore size as the erosion mechanism advances [16]. The integration of highly degradable materials, obtained by chemical modification of purified hyaluronan (HA), namely HYAFF11®, formed by the partial or total esterification of the carboxyl groups of glucuronic acid with different types of alcohols – provides the opportunity to affect directly the cell activities, either favouring or, conversely, inhibiting the adhesion of certain cell types [17][18][19]. Here, partially esterified HYAFF11® with reduced hydrophilic, negatively charged, carboxyl groups along the polymer backbone, - esterification degree equal of 75% - has been selected for its optimal hydrophilic/hydrophobic character which confers an adequate biological recognition, without drastically penalizing the structural integrity of the composite scaffold at the preliminary stage of the culture [20]. Finally, either PLA fibres or bioactive ceramic particles were added to the polymer matrix in order to satisfy specific structural requirements of scaffolds for load bearing applications.

In this work, we focus on the evolution of morphology and degradation properties of proposed composites for underlining the contribution of single material phases and their

peculiar chemical and physical properties on the dynamic changes of scaffold features within simulated *in vivo* conditions.

Materials and Methods

Materials and scaffold preparation

Poly ε-caprolactone pellets (MW 65 kDa, ρ= 1.13 g/cm^3 Aldrich) were dissolved in a solvent mixture to form a solution by stirring for 2h at 40°C. Two different solvents were used, respectively, tetrahydrofurane (Sigma Aldrich, Italy) and dimethylsulfoxide (Sigma Aldrich, Italy) by 80/20 weight ratio. A benzyl ester of hyaluronic acid with 75% of esterification degree (HYAFF11®-75p – ρ= 1.387 g/cm^3 [21]) supplied by Fidia Advanced Biopolymers in powder form, was then mixed to the polymer solution imposing a PCL/HYAFF11® weight ratio equal to 80/20.

Depending on scaffold type, NaCl crystals (Fluka) with specific size ranges (212-300 µm or 300-500 µm) were employed as templating agent by using different PCL/NaCl volume ratio. Furthermore, a mixture of $Ca_2NaK(PO4)_2$ (CSPP) and, monocalcium phosphate monohydrate (MCPM) supplied by the Technical University of Catalunia (UPC) under the name of R-cem or polylactid acid fibres (PLA - 75/24 dtex) supplied by Sofradim have been used as reinforcing agent.

Three different PCL and HYAFF11® based composite scaffolds typologies were prepared via phase inversion and salt leaching technique, labelled respectively as PH, PHR and PHF. The PH type was developed as from the PCL/HYAFF11® solution described above. Sodium chloride (NaCl) crystals, in the 212-300 µm size range, were then incorporated as templating agent into the polymer solution by using a PCL/NaCl volume ratio of 9/91 v/v. The mixture was placed into Teflon moulds reproducing the final dish shape, 5mm as diameter, of the scaffold for *in vitro* degradation tests. Finally, ethanol washings for 24h at room temperature were performed to completely extract the

used solvents whereas daily washing in bi-distilled water for 7 days were used to leach out NaCl crystals as well as to remove other contaminants.

Filler-loaded scaffolds (PHR) have been prepared as previously described, by further adding the R-cem ceramic powder to the PCL solution by using a PCL/R-cem weight ratio equal to 80/20. As a precautionary measure, R-cem powder and NaCl crystals were premixed before the introduction into the polymer solution to minimize the cluster formation.

Finally, fiber reinforced composite scaffolds (PHF) were obtained by combining the phase inversion/salt leaching and filament winding technology as described elsewhere [22]. Briefly, PLA fibres impregnated through the PCL/HYAFF11® solution, were wound on a polypropylene tubing coated stainless steel mandrel with 1 mm of diameter by using a specific winding parameter set (winding angle WA=45°, winding pitch WP=500μm). In this case, a less viscous polymer solution by changing the PCL/solvents (12/88 wt/wt) and the PCL/NaCl ratios (32/68 v/v) was selected in order to optimize the fibre/matrix adhesion, maintaining the same PCL/HYAFF11 ratio. Moreover, NaCl crystals with bigger sizes (300-500 μm) were used to minimize the effects of crystal fragmentation on the pore size, expected during the process. Once tubular shaped scaffold was obtained, conventional procedures involving ethanol and water washings, for 24 hours and 7 days, respectively, were employed. Cylindrical samples with 5mm as outer diameter and 10 mm as height were used for porosity investigations (n=5) while dish shaped samples, thickness of 3 mm, for degradation tests (n = 4).

Morphological investigation by SEM/FESEM

Scaffold morphology was investigated via Scanning Electron Microscopy using a scanning electron microscope (Stereoscan 440, Leica, UK). Briefly, specimens were

fractured in liquid nitrogen using a razor blade along preferential directions, parallel and perpendicular to the surface, respectively. The resulting transverse and longitudinal sections were gold-coated under vacuum by using an automatic coating sputter set at 15 mA for about 20 minutes (Emiscope SC500, Italy). The porosity was assessed in terms of pore size, shape and spatial distribution by images at different magnifications. Further investigations on the scaffold morphology have been performed with the support of field emission scanner electron microscopy (FE-SEM, FEI Quanta200, The Netherlands) able to recognize material phases with different chemical and physical properties by the detection of back scattered (BSE) electrons and secondary electrons (SE) at low acceleration voltage (4kV).

Quantitative µ-tomographic analysis

The samples were scanned using a SkyScan 1072 micro-CT desk scanner supported by micro-tomographic reconstruction software (Skyscan) [23][24]. The reconstruction of the three-dimensional objects was achieved through a serial reconstruction of cross sections or 2-D slice maps [20]. The output format for each sample was 300 serial 1024 ×1024 bitmap images with a resolution of 10.14 µm. After the serial reconstruction, the stack of the 2-D slice maps was elaborated to construct a realistic view of the 3D-object with possibilities to "rotate" and "cut" the object model through dedicated software (SkyScan pack– Belgium) as illustrated by Sun et al. [25]. By the accurate adjustment of brightness and image contrast and the manipulation of the grayscale thresholds, a 3-D model of the positive (*direct reconstruction*) and negative spaces (*reverse reconstruction*) was obtained, on which to calculate basic morphological parameters such as porosity (i.e, porosity degree, pore size) and bulk structure (i.e, strut size and distribution). The detailed assessment of pore morphology in term of pore size and distribution was performed by CTan Skyscan software whereas the evaluation of strut

parameters was performed by ANT Skyscan software. Moreover, further morphometric parameters were evaluated to complete the scaffold morphology characterization: the anisotropy degree (DA) and the Structure Model Index (SMI) respectively – which refer to preferential pore orientations, density and pore interconnection [26]. High DA values (generally over 1) indicated high anisotropy of the trabecular structure [27] where low SMI values usually referring to poor interconnection degree of porous network [28]. Finally, further analysis on individual 2-D slice permitted to distinguish single radiopaque phases through differences in contrast of local regions, offering an estimation of the spatial distribution of inclusions and reinforcing elements within the polymer matrix.

Degradation studies

a) In vitro *degradation assays*

In vitro degradation studies were carried out in a simulated body fluid (SBF) at a controlled temperature of (37±1)^{o}C. SBF was prepared by dissolving the reagents NaCl, $NaHCO_3$, KCl, $K_2HPO_4 \cdot 3H_2O$, $MgCl_2 \cdot 6H_2O$, $CaCl_2 \cdot 2H_2O$ and Na_2SO_4 into distilled water, as described by Kokubo et al [29]. The solution was buffered to pH 7.25 at 37 ^{o}C with tris(hydroxy-methyl)aminomethane and hydrochloric acid. Samples were immersed in SBF solution for time periods of 1, 4 and 8 weeks. The ratio of SBF volume to polymer mass was 1:100. The medium was not changed over the whole testing period. After a given time, the samples were extracted from the solution, rinsed gently with distilled water and left to dry at 37 $^{\circ}$C to a stable mass.

b) Mass loss measurements

The mass loss during immersion in SBF was calculated as

$$\text{Mass loss } [\%] = [(m_0 - m_1)/m_0] \times 100$$

where m_0 and m_1 are the masses of the samples before and after degradation, respectively. At least 4 samples per data point were measured.

c) DSC analysis

DSC measurements were performed with a TA Instrument model DSCQ1000 equipped with a liquid nitrogen cooling unit. The instrument was calibrated using indium and sapphire standards. All measurements were performed in a helium atmosphere using standard crimped aluminum pans. Samples, with average weights of 9.2–10.8 mg, were scanned at a heating rate of 10 ^{o}C min^{-1}. The glass transition temperature, Tg, was measured at the mid-point of the heat capacity inflexion point. The crystallization temperature, Tc, and melting temperature, Tm, were determined from the peak value of the respective endotherms and exotherms. The degree of crystallinity (Xc) was evaluated according to the following equation:

$$Xc\ \% = (\Delta H_m/\Delta H^o)\ X\ (100/w)$$

Where w is the weight fraction of PCL or PLA in the composite, ΔH_m is the measured enthalpy of melting and ΔH^o is the enthalpy of melting of a 100% crystalline (PCL 139.5 J/g) [30] and (PLA 93 J/g) [31]

d) TGA analysis

Thermal gravimetric analysis (TGA) was performed on a TA Instrument Q 500 under nitrogen atmosphere, from room temperature up to 700^{o}C, with a heating rate of 10^{o}C/min.

e) Raman spectroscopical analysis

A visible Raman Microscope Spectrometer (Nicolet Almega XR; laser 532 nm; laser power level: 100%; exposure time 30 sec; spectrograph aperture: 50 μm pinhole) was used to emboss changes in chemical structure of the scaffolds, after the degradation studies.

Results

Morphology

The morphology of the three composite scaffolds was first assessed by scanning electron microscopy (SEM) (Figs.1 and 2). In each case, high structural porosity, characterized by a bimodal pore size distribution, was observed. In the case of PH and PHR, cross-section images indicate a homogeneous spatial distribution of macropores of undefined shape and with sizes ranging from 150 to 500 micrometers (Fig.1 A-B). In the case of PHF scaffolds (Fig.1C), a more ordered structural organization is observed, with a well-defined arrangement of pores between adjacent fibres. PLA fibres are well integrated into the PCL porous matrix and appear to influence pore morphology. In all cases, micropores with sizes of *ca* 10 μm may be easily recognized, both in the bulk and on the scaffold surface (Fig 2A-B). Marked differences in micro- and macropore morphology are also apparent on comparing scaffolds with and without fibres. More specifically, a reduction in macroporosity as well as concomitant increase in microporosity have been revealed in the case of PHF, ascribable to the different amount of templating agent and polymer solution concentration used during the preparation. A more accurate investigation of scaffold morphology by FESEM allowed investigation of the distribution of different polymeric and ceramic phases into the scaffold matrix as a function of the chemical and physical properties. Topographic images of scaffolds (Fig. 3A - square) highlight the presence of the HYAFF11® hydrophilic phases (dark grey) embedded in the PCL hydrophobic matrix (light grey). The lower brightness of the Hyaff11 phases arises from the higher electron density of polymer due to the presence of benzylic groups, which cause higher scattering of secondary electrons compared to the PCL.

Higher magnification images (Fig. 3B) show the distribution of R-cem calcium phosphate particles with micrometric and sub-micrometric sizes, and their tendency to form micrometric clusters into the polymer matrix.

A quantitative investigation of scaffold morphology was carried out using microCT for all scaffold types (Fig. 4). First, the stack of X-Ray images radiographs was rendered as planar 2D slices (Figs 4, right side) in order to describe the scaffold architecture and to correlate structural differences with chemical composition changes. These slices confirm the preliminary indications obtained by SEM regarding pore size and homogeneous spatial distribution of pores. By comparing 2D slices from PH, PHR and PHF scaffolds (Fig.4, right side), the presence of localized domains with different radiopacity as a function of material density are recognized. In Fig 4, white regions indicate pores, whereas slightly contrasted regions (cyan regions) identify the PCL matrix, which shows a lower susceptibility to X-ray adsorption due to its reduced density. In turn, blue and orange regions are representative of HYAFF11® inclusions and calcium phosphate particles, respectively, as a function of the increasing material density.

Afterwards, the volume rendering (Fig.4, left side) was carried out to assess basic porosity parameters in the three-dimensional space. Typically, by converting the slices in "*black and white*" images, a loss of information on the composite materials phases can occur. However, this was not limitative in the case of the quantitative pore investigation performed which has been referred only to the calculation of objects on macrometric scale (i..e, macropores, filler cluster, fibre bundle). In Table 1, a summary of porosity features for the different scaffolds is reported. Porosity degrees ranged from 63.1 to 82.8 %, pore sizes from 170.5 to 230.4 μm, the anisotropy degree from 0.1 to 0.226, moving from fiber reinforced scaffolds to fibreless one. According to the difference in scaffold porosity, the SMI values change ranging from 0.951 to 2.002.

Degradation studies

a) In vitro *mass loss*

The changes in mass loss of the scaffolds as a function of degradation time are shown in Fig. 5. After 1 week of immersion in SBF, the mass loss was comparable for all three materials and less than 2%. After 4 weeks of immersion in SBF, a linear weight loss was observed for all the composites. The highest weight loss – 15.5% - was observed for PHR whereas the lowest – 10% - for PH scaffold. During the next 4 weeks, the degradation rate of PHR decreased, so reaching, after 8 weeks degradation, comparable mass losses at *ca*17% for all composites (Table 2).

b) Raman Spectroscopy

Fig. 6 illustrates Raman spectra of PH (Fig. 6A), PHR (Fig. 6B) and PHF (Fig. 6C) scaffolds before and after 8 weeks of *in vitro* degradation. Bands at 1458 and 2940 cm^{-1} are assigned to carbon – hydrogen (C-H) stretching vibrations in aliphatic chains of PLA and hyaluronan. The 1740 cm^{-1} band is associated with vibration of carbonyl groups in lactones. Peaks at 3060, 3080 (valence vibration of C-H band in benzene), and at about 1600 cm^{-1} (acryl group) are from aromatic ring vibrations. Ester group vibrations are evident as a pair of bands at 1000 – 1100 cm^{-1} and 1100 – 1300 cm^{-1}.

The presented spectral data provide evidence of the hydrolysis of ester bonds in hyaluronic derivatives. As a result, benzoic acid came into the solution, leading to changes in pH during degradation. The peaks assigned to aromatic compounds disappeared after 1 week of degradation in the case of PHF and PH scaffolds and after 4 weeks for PHR scaffold.

c) DSC measurements

DSC thermograms of all the scaffold typologies are shown in Fig.7A-C. Additionally, the curves regions showing glass transition are presented in Fig.7D-F. The values of characteristic temperatures (T_g, T_m) as well as enthalpies (of melting and crystallization) and the crystallinity degree are summarized in Table 2. The Tg temperatures of microporous PCL/HYAFF11® -based scaffolds are close to the values quoted for PCL, i.e. -60°C (Table 2). The T_g of PLA of about 55°C [32] cannot be exactly determined for PHF scaffolds, as it is very close to the T_m of PCL (Fig. 7C). Relatively minor changes were observed in T_g values over 8 weeks of immersion in SBF for all studied materials. All the thermograms displayed one sharp melting peak at around 60°C (Fig.7A-C) associated with the melting of PCL crystalline phase. The total amount of the crystalline phase of PCL segment increased during soaking in SBF for all samples (Table 2). The melting temperature remained almost unchanged during *in vitro* soaking. In addition, for PH and PHR scaffolds, a second melting peak at 143-149.5°C appeared after 1 and 4 weeks immersion in SBF, respectively (Fig. 7A,B). In the case of PH-based scaffold, a small and sharp peak located at about 162°C and associated with the melting of PLA was also observed (Fig. 7C).

d) TGA measurements

TGA curves of PH and PHR showed a two-step degradation process (Fig.8A,B) whereas for PHF three stages of degradation were observed (Fig.8C). Weight losses and decomposition temperatures for the composites after different periods of immersion in SBF are summarized in Table 3. The maximum temperature (peak) of the first stage thermal degradation related to the HYAFF11® decomposition, ranged from 222.8 °C to 255.0°C. The second and third stage of thermal degradation observed in the temperature range of 333 °C - 361 °C, and 399.6 °C - 403.8 °C, can be attributed to the decomposition of PCL and PLA macromolecules, respectively. Initial samples of PH and PHR showed a weight loss of 15% and 14%, respectively, in the first step. As the

HYAFF11® content of these composites varies from 20% in PH to 17% in PHR, a correlation can be drawn between HYAFF11® content and weight loss. During soaking in SBF, the weight loss in the first step of degradation decreased and, after 8 weeks, only one step degradation at the temperature range 292-499°C was observed for PH. For PHR the weight loss dropped to 4% in the first stage degradation after 4 weeks immersion in SBF, whereas, after 8 weeks, a 6% weight loss was observed. The same situation was also observed for the PHF scaffolds. After 1 week soaking in SBF, a three-step degradation process was observed (Fig.8C). The weight loss decreased from 9% to 7% in the first degradation step, but increased from 8% to 10% in the second. After 4 weeks of *in vitro* degradation, the weight loss further increased to 13% in the second step of thermal degradation. After 8 weeks immersion only a one step degradation process, associated with PCL thermal degradation, was observed.

Discussion

The current challenge in scaffold design is to fabricate reproducible bioactive and bioresorbable 3D scaffolds with tailored porosity and pore morphology, capable of maintaining structure integrity for a predictable period, even under load-bearing conditions. Through the time-controlled resizing of pores which occurs during degradation, materials with a predictable degradation rate may guarantee greater penetration of extracellular substance, improve the nutrient/metabolites exchange and offer a better connection between neighbouring cells, so encouraging and promoting the growth of new tissue. Apart from creating the physico-chemical environment and the structural integrity required for tissue regeneration, scaffolds also should act as a local regulator to control the release of signals, preferably without the use an additional drug carrier [33].

Here, three biodegradable scaffolds, based on PCL as a major component, and with tailored microstructure and multi-scale degradation rates, were investigated to estimate the dynamic changes occurring in the pore network during the resorption. Recently, an upward trend in PCL use in biomaterials for tissue engineering has been observed. This is due to the high processability of such materials into composite structures with superior mechanical and biocompatible properties compared to the polymer on its own [34][35][36].

Three different typologies of composite scaffolds have been proposed by the integration into the PCL matrix of different material phases: Hyaff11, as a hydrophilic cue; R-cem (particles) as reinforcement systems by using conventional phase inversion/salt leaching technique alone (i.e, PH, PHR); or incorporation of PLA long fibers by filament winding technique (i.e, PHF). All scaffold prototypes showed a bimodal porosity, characterised by macropores arising from salt crystal dissolution (Figure 2), and micropores formed by the controlled removal of solvent *via* non-solvent exchange (Figure 2). These characteristics assure an open-pore network, highly capable of supporting cell adhesion and proliferation, preserving the correct and requisite fluid transport, and sustaining the external mechanical stress until the regeneration of new functional tissue is completed. The investigation of morphology by X-ray micro-computed tomography (microCT, or μCT), whose use has recently been adopted for the study of soft materials and natural tissues [37][38] in place of invasive intrusion-based techniques [39], allowed a quantitative assessment of scaffold porosity features (pore size, structural porosity and degree of anisotropy) as summarized in Table 1. The data here clearly show the contribution of polymer phases with different chemical and physical properties on determining the final pore morphology of the scaffold. Porosity and pore sizes of PH scaffolds are firstly affected by the response of the HYAFF11® phases to the water retention, leading to a slight underestimation of pore sizes (around

170 μm) due to swelling of the hydrogel through absorption of environmental moisture. The moderate increase of pore sizes in the case of PHR scaffolds may be explained by the effect of rigid R-cem calcium phosphate particles, which partially constrain the water induced swelling of the HYAFF11® phases. However, it should not to be discounted that the reduced loss of R-cem particles due to the high water retention of the hydrogel during the drying of the scaffold may also contribute to this effect. In the case of PHF scaffolds incorporating PLA fibre, a drastic decay of the porosity degree, from 81.7% to 63.1%, was observed, when a smaller weight amount of sodium chloride crystals was used in order to reduce the solution viscosity, and thus optimize the fibre/matrix adhesion, during the winding process.

Accurate microCT investigation also affords the opportunity to identify the spatial distribution of polymer phases with different chemical properties and so evaluate their contribution on the composite degradation behaviour. In particular, by regulating the voltage/current characteristics, microCT enabled the identification of distinct single phases within the composite (Fig. 4), and their spatial distribution. In turn, this enabled an informed optimization of the composite preparation process. By comparison domains with different radiopacity, it has been possible to identify the contributions of:

I) a non-homogeneous spatial distribution of calcium phosphate particles in PHR scaffolds with the clusters formation (orange region), and

II) more dense polymer phases of HYAFF11® (blue region), which seem preferentially to cover the boundaries of the ceramic particles due to the adsorption of the water molecules during the scaffold preparation process.

Our studies on *in vitro* hydrolytic degradation of PCL/HYAFF11® -based scaffolds indicate the strong influence of the extent, interrelationship and distribution of the phases of the various polymer components – indeed, the influence of what might be considered the "design" generated by these chemically distinct phases. Although all the

polymeric components (i.e., PCL, PLA, and HYAFF11®) of the composites studied undergo degradation *via* random hydrolytic chain scission of the ester linkage, their individual rates of degradation are considerably different [40][41]. The most significant differences in mass loss were observed after 4 weeks of immersion. It is assumed that most of the mass loss at the first 4 weeks of degradation was due to degradation products of HYAFF11®-p75 leaving the system by dissolving into the aqueous medium [42]. The decreasing amount of weight loss attributable to thermal decomposition of HYAFF11® segments [43], as immersion time in SBF increases, seems to confirm this. This is also in good agreement with Raman spectroscopy analysis, which showed an absence of bands associated with aromatic ring vibrations in all those composite samples examined after either 1 or 4 weeks immersion in SBF. The rapid degradation rate of HYAFF11®-p75 correlates very well with the findings of Avitabile *et al* [44], who reported that HYAFF11®-p75 based implants were fully resorbed after 15 days implantation in rabbit.

The higher degradation rate of PHR composite may be due to the presence of the highly hydrophilic R-cem particles. The accelerating effect of various ceramic fillers on PCL degradation rate has been previously reported [45][46]. Hydrophilic fillers can facilitate water absorption, leading to faster degradation of HYAFF11® macromolecules, explaining why PHR composites show the highest mass loss of all the composites studied during the first 4 weeks of immersion in SBF. The mass loss can arise from the diffusion of the ceramic filler from the sample into solution, so creating voids and microcracks within the sample. After this initial period, its degradation rate clearly diminished (Fig.5).

A slower degradation rate directly results from an increased degree of crystallinity, as revealed by DSC analysis (Table 2). Polyester degradation starts with water uptake [32].The diffusion of water into loosely packed amorphous regions is

much easier than its ingress into crystalline domains, and accordingly the first stage of hydrolytic degradation is located in the amorphous region of the sample. The initial degree of crystallinity for PH was more than 10% higher than that for PHR and PHS composites. Also, the crystallinity of PH increased by 10% after immersion in SBF for 1 week (Table 2), whereas for the crystallinity of PHR and PHF samples remained unchanged over the same period. The slow increase in crystallinity enabled faster diffusion of water into the PHR and PHF matrices during the next 3 weeks of soaking in SBF, and thus faster hydrolysis leading to higher mass loss (Fig.5). As degradation proceeds by random scission of ester bonds, the remaining chain segments gain more space and mobility, leading to reorganization of the polymer chains and an increase in crystallinity. In the case of PH and PHR, shorter more labile polymer chains retained in the polymer matrix generated a biphasic crystalline phase, manifesting itself in the presence of additional melting peaks at around 147^{o}C, which appeared after immersion in SBF (Figs. 6 A-B).

.

Conclusion

Three biodegradable scaffolds based on a PCL and HYAFF11® matrix, with tailored chemical and physical properties, were developed for bone and/cartilage tissue regeneration. The combined use of SEM and computer microtomography (mCT), supported by digital image analysis, enabled a non-destructive investigation of the diverse porous microstructures of the proposed scaffolds. This investigation demonstrated the contribution of single composite phases to the basic morphological features. Furthermore, *in vitro* degradation studies have demonstrated the need to reach a compromise between the material chemistry and the composite structural design to predict *ab initio* the dynamic changes which may occur as the hydrolytic degradation

mechanism progressively evolves, paving the way for a more informed use of polymeric composite scaffolds with multiscale degradation in bone tissue regeneration.

Acknowledgements

This study was financially supported by the IP STEPS EC project, FP6-500465.

References

[1] Ciapetti G., Ambrosio L., Marletta G., Baldini N., Giunti A. Human bone marrow stromal cells: *In vitro* expansion and differentiation for bone engineering. Biomaterials 2006;27:6150–6160;

[2] Guarino V., Causa F., Ambrosio L. Bioactive scaffolds for connective tissue regeneration. Expert Rev. Med. Devices 2007;4(3):406-18.

[3] Savarino L., Baldini N., Greco M., Capitani O., Pinna S., Valentini S. et al. The performance of poly-e-caprolactone scaffolds in a rabbit femur model with and without autologous stromal cells and BMP4. Biomaterials 2007;28:3101–3109;

[4] Hak-Joon Sung, Carson Meredith, Chad Johnson, Zorina S. Galis - The effect of scaffold degradation rate on three-dimensional cell growth and angiogenesis - Biomaterials 25 (2004) 5735–5742.

[5] Seal B.L., Otero T.C., Panitch A. Polymeric biomaterials for tissue and organ regeneration. Mater Sci Eng: R: Rep 2001;34:147–230.

[6] Kohn J.R.L. Bioresorbable and bioerodible materials. In: Ratner BD, Hoffman AS, Schoen FJ, JE L, editors. Biomaterials science: an introduction to materials in medicine. New York: Academic Press; 1996. p. 64–72.

[7] Manjubala I., Woesz A.,Pilz C., Rumpler M., Fratzl-Zelman N., Roschger P., Stampfl J. Biomimetic mineral-organic composite scaffolds with controlled internal architecture. J. Mat Sci: Mat Med 2005;16:1111 – 1119.

[8] Lu L, Garcia CA, Mikos AG. *In vitro* degradation of thin poly(dl-lactic-co-glycolic acid) films. J Biomed Mater Res 1999; 46:236–44;

[9] Miller RA, Brady JM, Cutright DE. Degradation rates of oral resorbable implants (polylactates and polyglycolates): rate modification with changes in PLA/PGA copolymer ratio. J Biomed Mater Res 1977;11:711–9;

[10] Santavirta S., Konttinen Y.T., Saito T., Gronblad M., Partio E., Kemppinen P., Rokkanen P. Immune response to polyglycolic acid implants. J Bone Jt Surg Br 1990;72:597–600.

[11] Andrew S.D., Phil G.C., Marra K.G. The influence of polymer blend composition on the degradation of polymer/hydroxyapatite biomaterials. J Mater Sci: Mater Med 2001;12:673–7.

[12] Chiari C., Koller U., Dorotka R., Eder C., Plasenzotti R., Lang S., Ambrosio L., Tognana E., Kon E., Salter D., Nehrer S. A tissue engineering approach to meniscus regeneration in a sheep model. OsteoArthr. Cart. 2006;14:1056-65.

[13] Kon E, Chiari C, Marcacci M, Delcogliano M, Salter DM, Martin I, Ambrosio L, Fini M, Tschon M, Tognana E, Plasenzotti R, Nehrer S. Tissue Engineering for Total Meniscal Substitution: Animal Study in Sheep Model. Tissue Eng Part A 2008;14(6):1067.

[14] Gabelnick HL. Biodegradable implants: alternative approaches. In: Mishell DR, editor. Advanced in human fertility and reproductive endocrinology: vol. 2: Long acting steroid contraception. New York: Raven Press; 1983. p. 149–73.

[15] Gunatillake PA, Adhikari R. Biodegradable synthetic polymers for tissue engineering.Euro Cells Mater 2003;5:1-16.

[16] Rezwan K., Chen Q.Z., Blaker J.J., Boccaccini A.R. Biodegradable and bioactive porous polymer/inorganic composite scaffolds for bone tissue engineering. Biomaterials 2006;27:3413–3431.

[17] Campoccia D., Doherty P., Radice M., Brun P., Abatangelo G., Williams D.F. Semisynthetic resorbable materials from hyaluronan esterification. Biomaterials 1998;19:2101–27.

[18] Turner N.J., Kielty C.M., Walker M.G., Canfield A.E. A novel hyaluronan-based biomaterial (Hyaff-11s) as a scaffold for endothelial cells in tissue engineered vascular grafts - Biomaterials 2004;25:5955–5964.

[19] Grigolo B., Roseti L., Fiorini M., Fini M., Giavaresi G., Aldini N.N., Giardino R., Facchini A. Transplantation of chondrocytes seeded on a hyaluronan derivative (hyaff-11) into cartilage defects in rabbits. Biomaterials 2001;22:2417–24.

[20] Mori M., Yamaghuci M., Sumitomo S., Takai Y. Haluronan-based biomaterials in tissue engineering. Acta Hystochem. Cytochem. 2004;37(1):1-5.

[21] Netti P.A., Ambrosio L., Nicolais L. - Thermodynamics of Water Sorption in Hyaluronic Acid and Its Derivatives in Polymeric drugs & drug delivery systems Editors: R M. Ottenbrite,SW Kim, 2000, CRC press

[22] Guarino V., Causa F., Taddei P., Di Foggia M., Ciapetti G., Martini D. et al Polylactic acid fibre reinforced polycaprolactone scaffolds for bone tissue engineering. Biomaterials 2008;29:3662.

[23] Guarino V., Ambrosio L. The synergic effect of polylactide fiber and calcium phosphate particles reinforcement in poly ε-caprolactone based composite scaffolds. Acta Biomat. 2008;4:1778-87.

[24] Darling L., Sun W. 3D Microtomographic Characterization of Precision Extruded Polycaprolactone Scaffolds. J Biomed Mater Res Part B: Appl Biomater 2004;70:311–317.

[25] Sun W., Lal P. Recent development on computer-aided tissue engineering—a review. J. Comp. Meth. and Programs in Biomedicine 2002;67(2):85-103.

[26] Hildebrand T, Rüegsegger P. Quantification of Bone Microarchitecture with the Structure Model Index. Comput Methods Biomech Biomed Engin. 1997;1(1):15-23.

[27] Ruegsegger P, Koller B, Muller R. A microtomographic system for the nondestructive evaluation of bone architecture. Calcif Tissue Int 1996;58:24–29

[28] Ohser J., Redenbach C., Shladitz K. – Mesh free estimation of the structure model index. Image Anal Stereol 2009; 28: 179-185.

[29] Kokubo T. Takadama H. Biomaterials 27 2006 2907-2915

[30] Coombes A.G.A., Rizzi S.C., Williamson M., Barralet J.E., Downes S., Wallance W.A. Precipitation casting of polycaprolactone for applications in tissue engineering and drug delivery. Biomaterials 2004; 25:315-325.

[31] Sarazin P., Roy X., Favis B.D. Controlled preparation and properties of porous poly(L-lactide) obtained from a co-continuous blend of two biodegradable polymers. Biomaterials 2004;25(9):5965-78.

[32] Södergard A., Stolt M. Properties of lactic acid based polymers and their correlation with composition Prog.Polym. Sci. 2002; 27:1123-1163

[33] Mouriño V., Boccaccini AR Bone tissue engineering therapeutics: controlled drug delivery in three-dimensional scaffolds. J. R. Soc. Interface 2010; 7:209-227

[34] Luciani A., Coccoli V, Orsi S, Ambrosio L, Netti PA. PCL microspheres based functional scaffolds by bottom-up approach with predefined microstructural properties and release profiles. Biomaterials 2008;29:4800-7.

[35] Marrazzo C., Di Maio E., Iannace S. Conventional and nanometric nucleating agents in poly(epsilon-caprolactone) foaming: Crystals vs. bubbles nucleation. Polym Eng Sci 2008;48:336-44.

[36] Guarino V., Causa F., and Ambrosio L. Porosity and mechanical properties relationship in PCL based scaffolds. J Appl Biomater Biomech 5, 149, 2007.

[37] Mawatari T., Miura H., Higaki H., Kurata K., Moro-oka T., Murakami T., Iwamoto Y. Quantitative analysis of three-dimensional complexity and connectivity changes in trabecular microarchitecture in relation to aging, menopause, and inflammation. J Orthop Sci 1999;4:431– 438.

[38] Lin A.S., Barrows T.H., Cartmell S.H., Guldberg R.E. Microarchitectural and mechanical characterization of oriented porous polymer scaffolds. Biomaterials 2003;24:481– 489.

[39] Gupta G., Zbib A., El-Ghannam A., Khraisheh M., Zbib H. Characterization of a novel bioactive composite using advanced X-ray computed tomography. Composite Structures 2005; 71:423–428.

[40] Göpferich A. Mechanisms of polymer degradation and erosion. Biomaterials 1996;17:103-114.

[41] E. Milella, E. Brescia, C. Massaro, P.A. Ramires, M.R. Miglietta, V. Fiori, P. Aversa " Physico-chemical properties and degradability of non-woven hyaluronan benzylic esters as tissue engineering scaffolds" Biomaterials 23 (2002) 1053-1063

[42] Milella E., Brescia E., Massaro C., Ramires P.A. Chemico-physical properties of hyaluronan-based sponges. J Biomed Mater Res 2000; 52:695-700.

[43] Tsuji H., Ono T., Saeki T., Daimon H., Fujie K. Hydrolytic degradation of poly(3-caprolactone) in the melt; Polymer Degradation and Stability 2005; 89:336-43.

[44] Avitabile T., Marano F., Castiglione F., Bucolo C., Cro M., Ambrosio L., Ferrauto C., Reibaldi A. Biocompatibility and biodegradation of intravitreal hyaluronan implants in rabbits. Biomaterials 2001; 22:195-200.

[45] Chouzouri G., Xanthos M. *In vitro* bioactivity and degradation of polycaprolactone composites containing silicate fillers Acta Biom. 2007; 3:745–756.

[46] Prabhakar R.L., Brocchini S., Knowles J.C. Effect of glass composition on the degradation properties and ion release characteristics of phosphate glass—polycaprolactone composites Biomaterials 2005; 25:2209–2218.

Captions to Figures

Figure 1: S.E.M. images of cross-sections of PCL/HYAFF11® -based composite scaffolds:. A) PH, B) PHR, and C) PHF.

Figure 2: Microporosity of PCL/HYAFF11® based composite scaffolds by SEM analysis. Micropores (A) along PH scaffold struts and (B) onto PHF outer surface.

Figure 3: Morphology of PCL/HYAFF11® based composite scaffolds by FE-SEM analyses. (A) Detection of hydrophilic HYAFF11® (*dark gray*) patches (by arrows) onto the hydrophobic PCL (*light gray*) architecture, (B) Distribution of R-cem particles in cluster form within the polymer matrix.

Figure 4: MicroCT analysis: 3D Rendering (*left*) and 2D slice maps of material phase density variations (*right*) of proposed PCL/HYAFF11® -based composite scaffolds: (A) PH, (B) PHR and (C)PHF.

Figure 5: Mass loss of the composite scaffolds as a function of degradation time in SBF solution.

Figure 6: Raman spectra of (A) PH, (B) PHR and (C) PHF scaffolds before and after degradation.

Figure 7: DSC thermograms of PCL/HYAFF11® composites before and after immersion in SBF. (A-D) PH, (B-E) PHR and (C-F) PHF.

Figure 8: Thermogravimetric curves of PCL/HYAFF11® composites before and after immersion in SBF. (A) PH, (B) PHR and (C) PHF.

Table 1. Porosity features obtained on the different composite scaffolds by the MicroCT analysis

Type	Total Porosity degree (%)	Average macropore sizes (10-500 μm)	Anisotropy Degree	Structure Model Index (SMI)
PHS2	81.7	170.4	0.215	1.947
PHRS2	82.8	198.7	0.226	2.002
PHF2	63.1	230.5	0.1	0.951

Table 2. DSC results for the composites after different time immersion in SBF

Type	Degradation time, weeks	Tg, °C	Tm_1, °C	ΔHm_1 J/g	ΔHc J/g	Tm_2, °C	ΔHm_2 J/g	Xc PCL, %	Xc PLA, %
PHS2	0	-59.8	62.4	71.1	33.3	-	-	59.8	-
	1	-60.1	63.4	88.4	42.6	147.6	1.3	75.8	-
	4	-61.0	61.6	84.9	55.3	149.5	4.1	82.7	-
	8	-61.0	63.4	94.0	60.8	147.6	2.6	90.3	-
PHSR2	0	-61.2	62.3	62.9	36.0	-	-	46.8	-
	1	-60.4	63.6	64.7	39.4	-	-	49.3	-
	4	-59.9	62.4	76.5	51.4	146.1	1.4	61.1	-
	8	-61.0	62.8	75.4	43.0	143.0	11.5	61.4	-
PHF2	0	-58.9	62.9	50.2	48.5	161.0	4.2	49.5	0.5
	1	-60.1	63.4	50.5	48.4	161.2	4.2	49.8	0.5
	4	-60.3	63.3	76.6	53.9	160.7	7.3	65.5	0.9
	8	-61.1	64.4	85.8	58.8	160.5	2.1	72.0	0.2

Table 3. Weight losses and decomposition temperatures for the composites after different time of immersion in SBF

Type	Degradation time, weeks	First degradation temperature (°C)			Weight loss, %	Second degradation temperature (°C)			Weight loss, %	Third degradation temperature (°C)			Weight loss, %
		Start	Peak	End		Start	Peak	End		Start	Peak	End	
PHS2	0	177	233	303	15				-	303	400	504	77
	1	142	242	296	13		-		-	296	400	507	80
	4	154	222	292	7				-	292	402	529	86
	8	-	-	-	-				-	292	404	499	91
PHRS2	0	177	239	311	13				-	311	401	576	69
	1	150	243	300	14		-		-	300	403	548	67
	4	161	231	269	4				-	269	402	500	84
	8	148	254	286	7				-	286	399	510	76
PHF2	0	174	233	265	9	265	311	334	8	334	403	490	75
	1	199	247	266	7	266	308	339	10	266	308	339	75
	4	-	-	-	-	263	339	352	13	352	409	501	85
	8	-	-	-	-	-	-	-	-	271	409	479	99

Figure 1

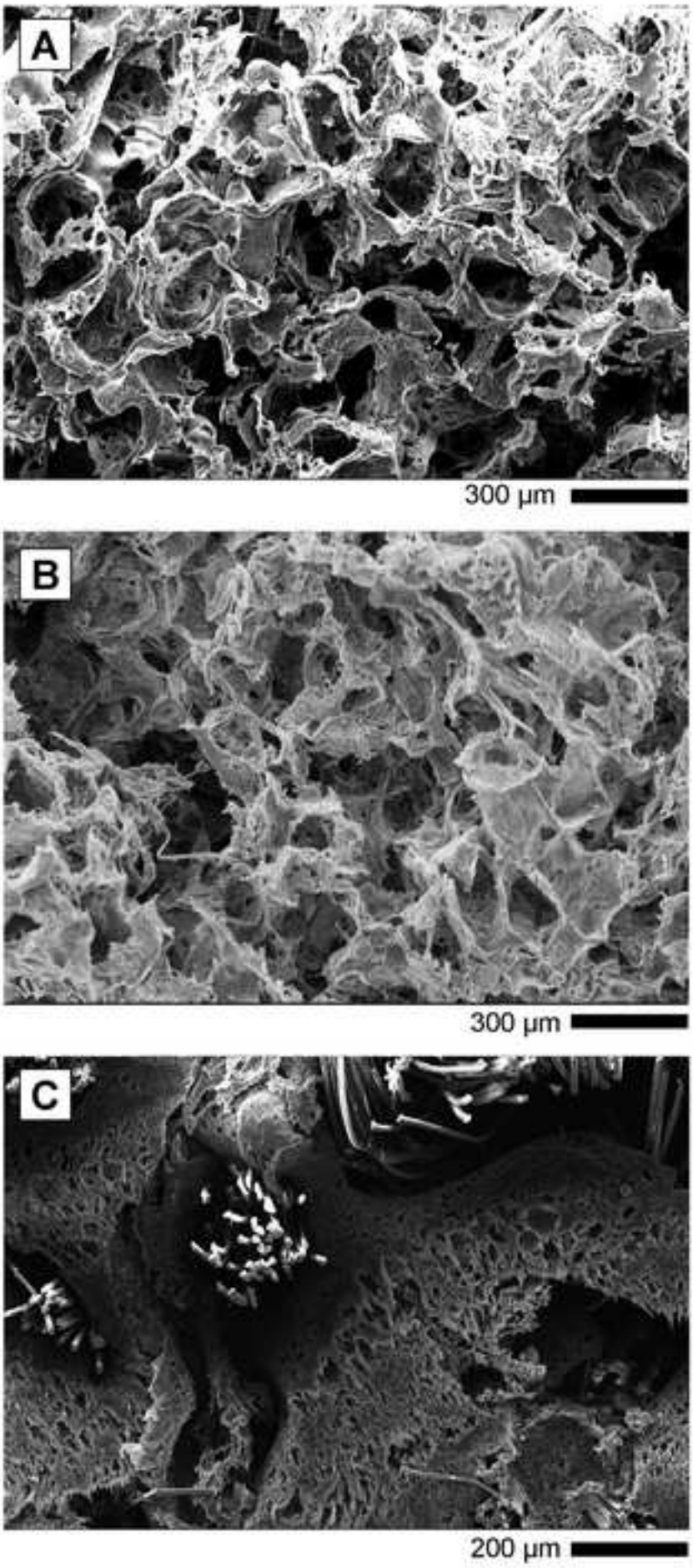

Figure 2

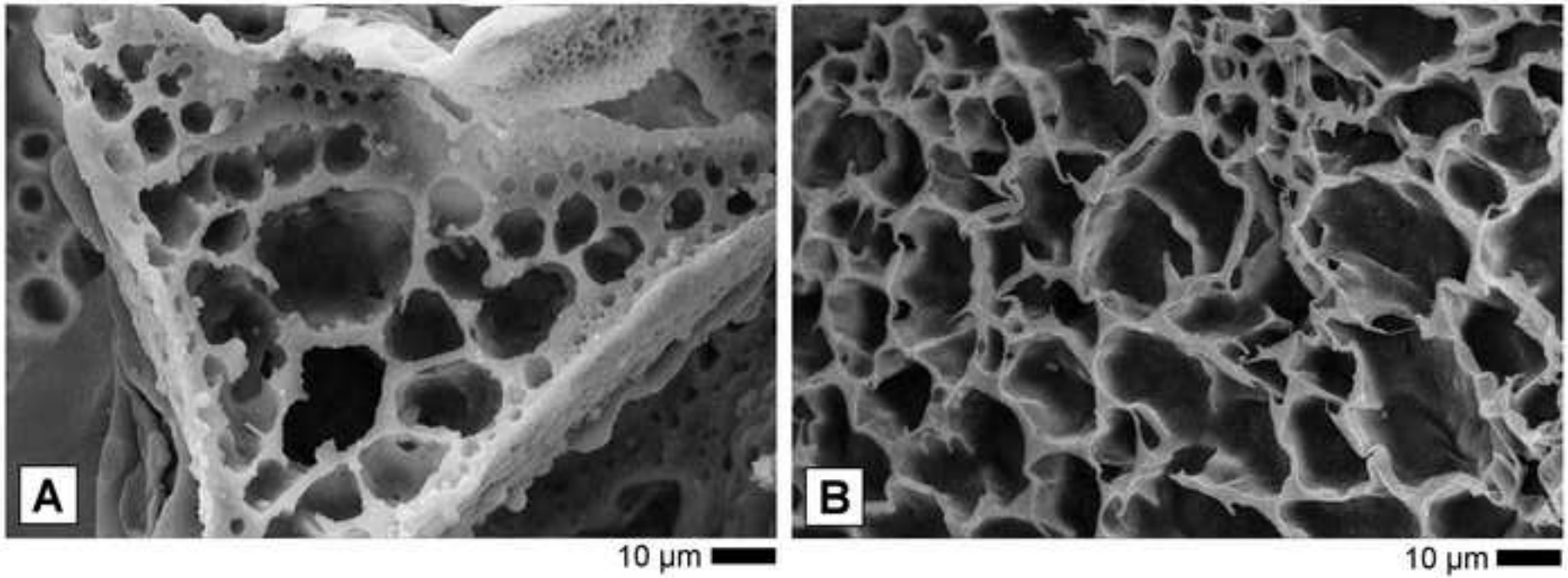

Figure 3

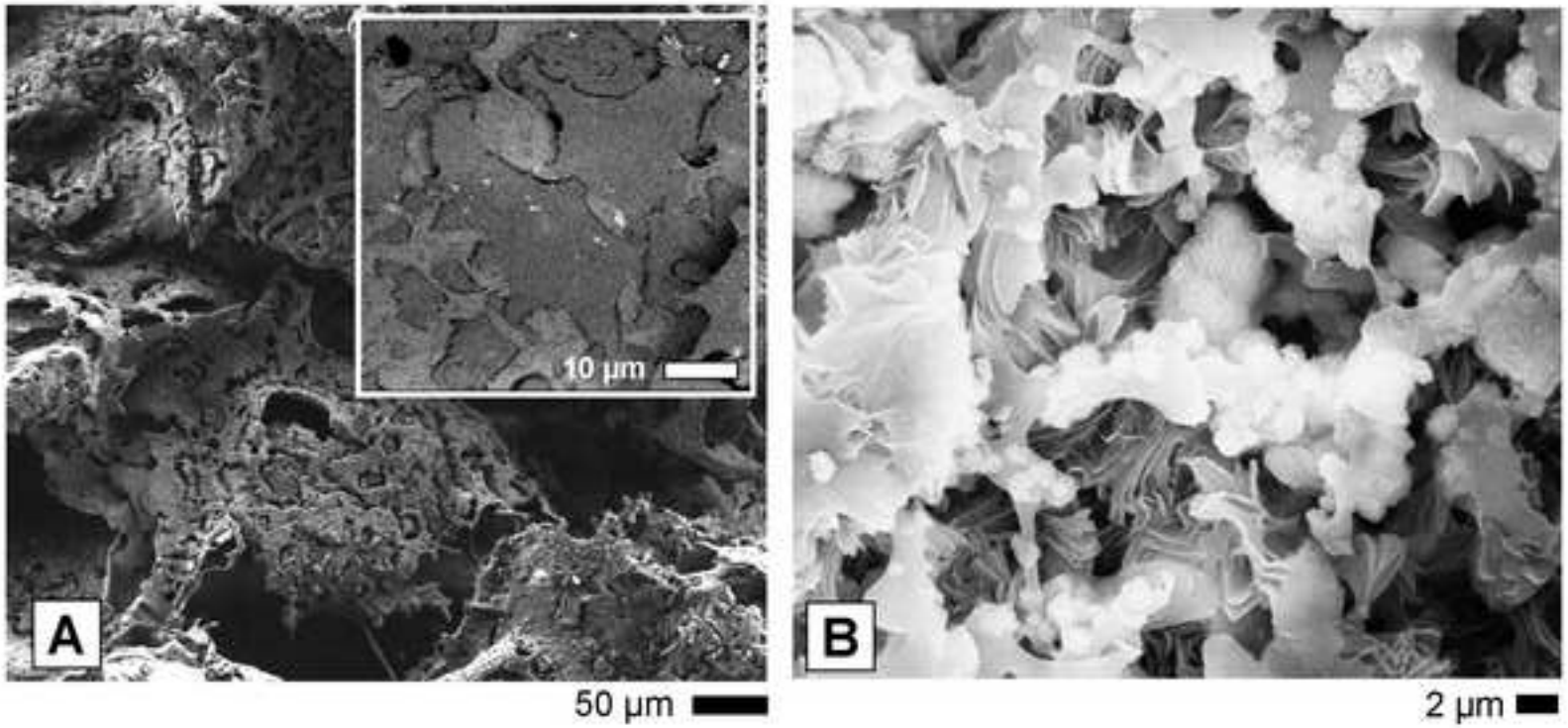

Figure 4

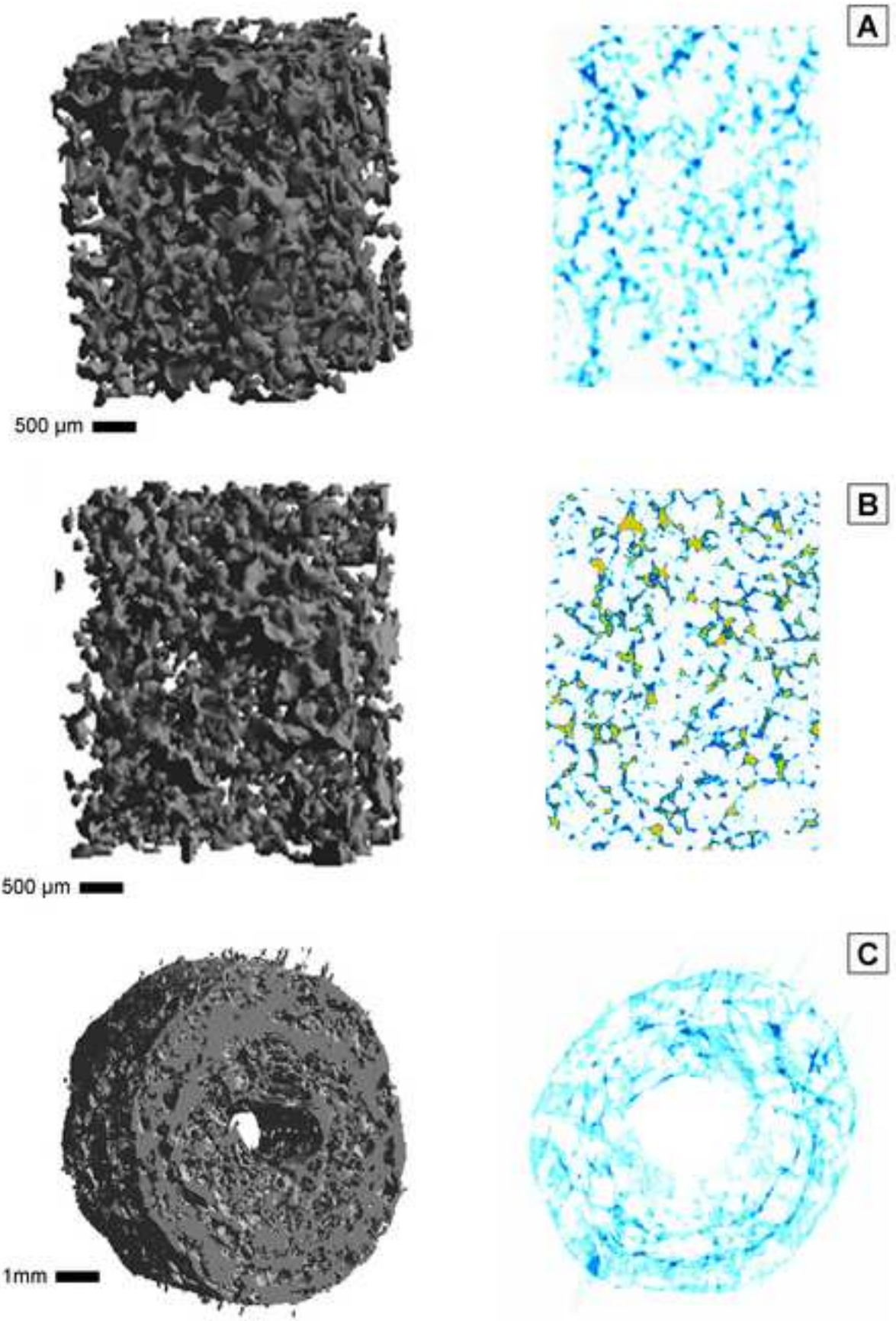

Figure 5

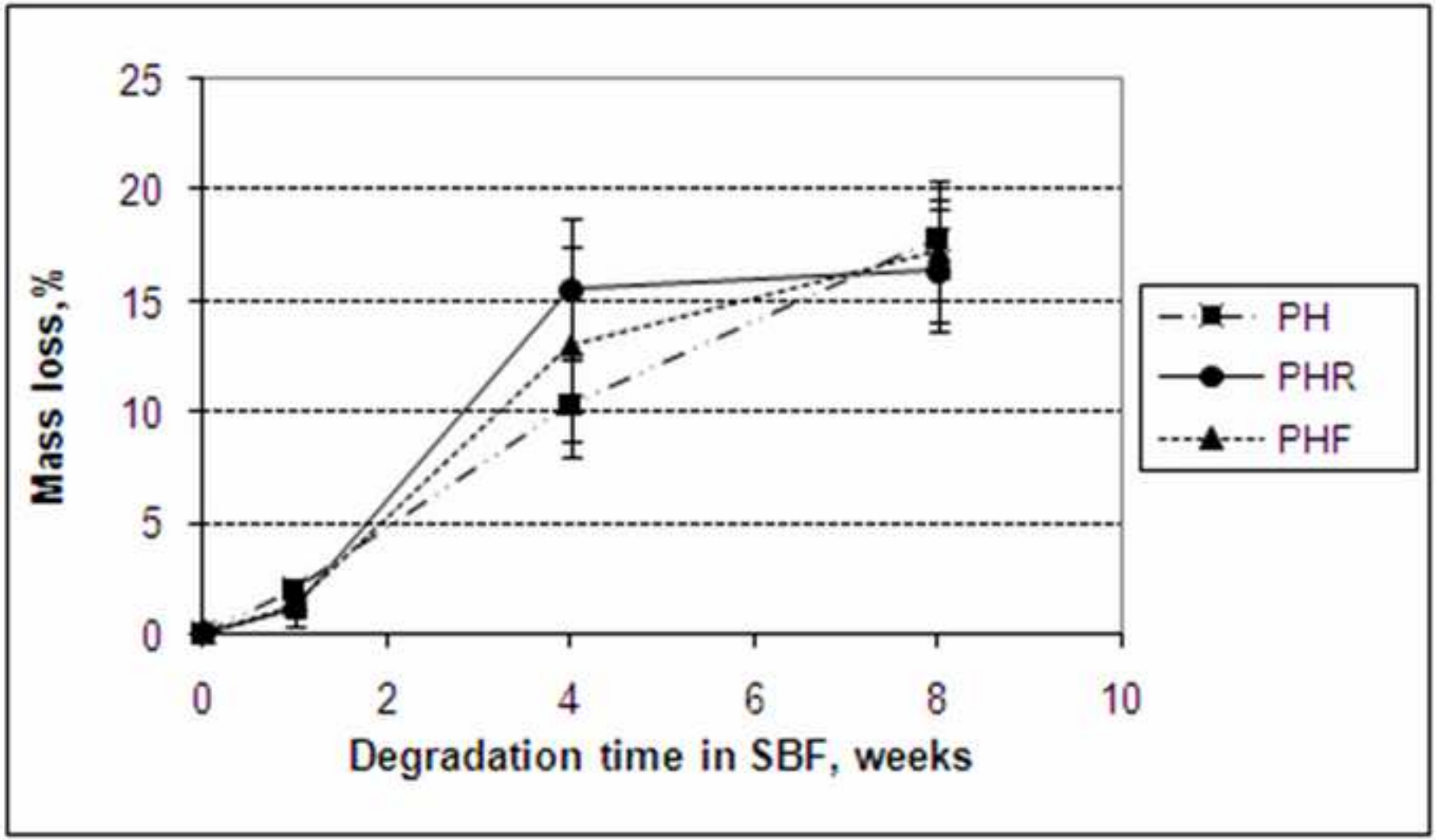

Figure 6

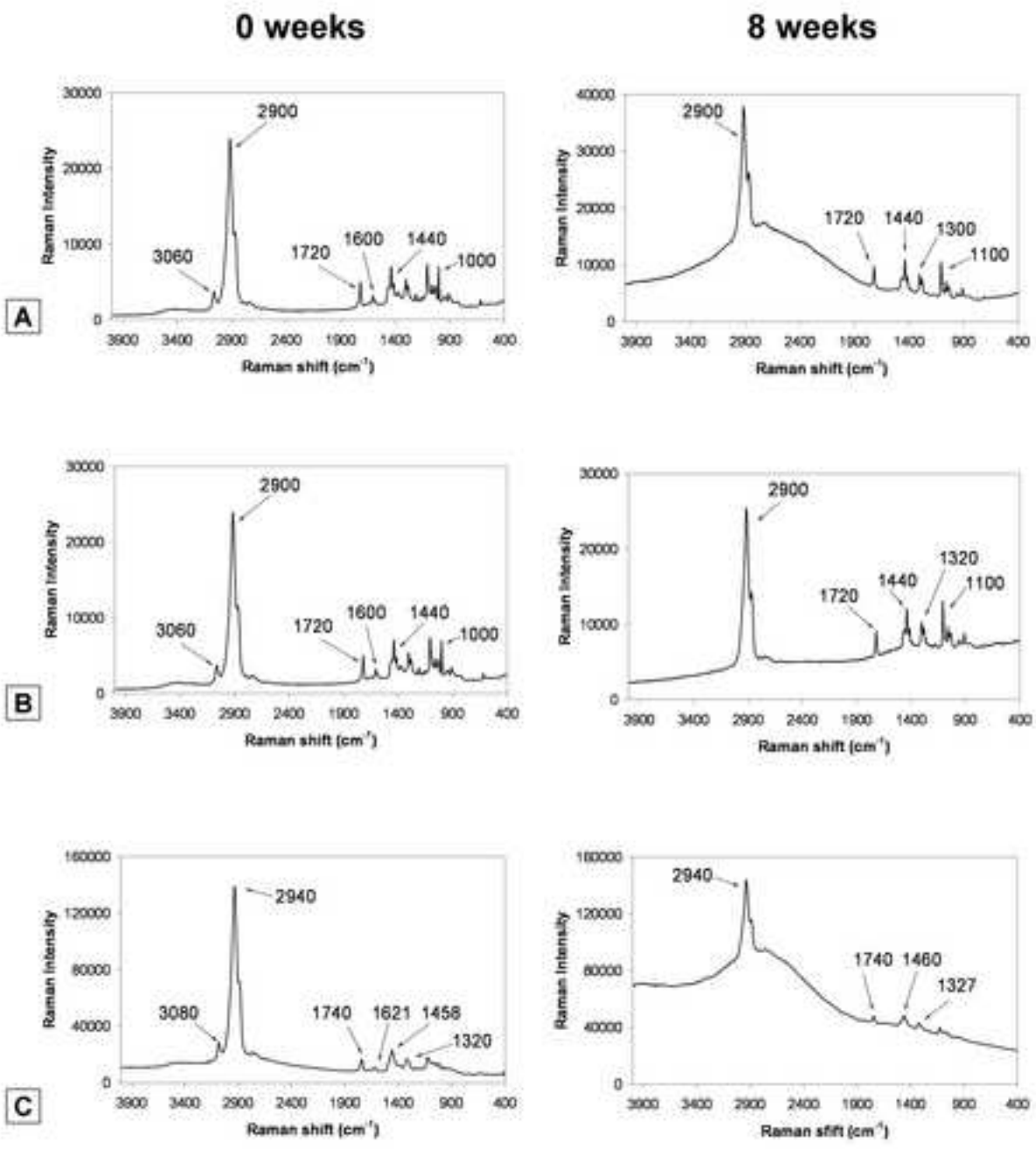

Figure 7A,B,C

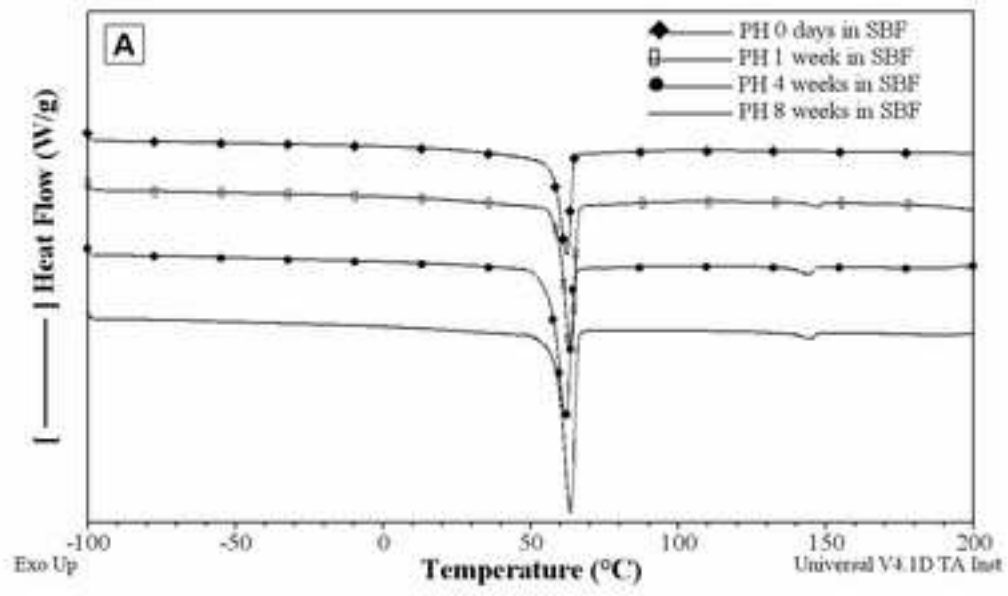

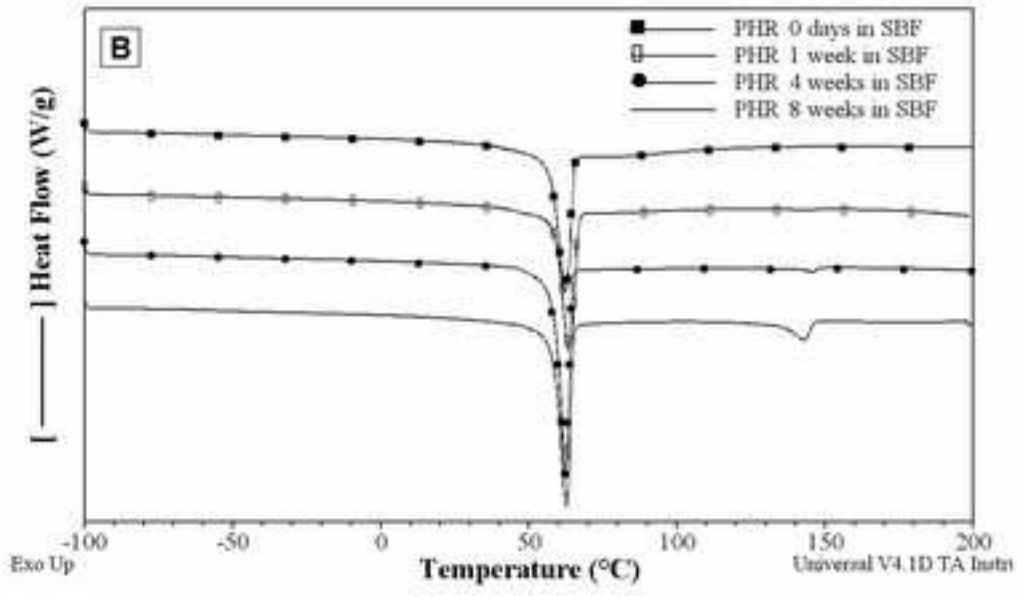

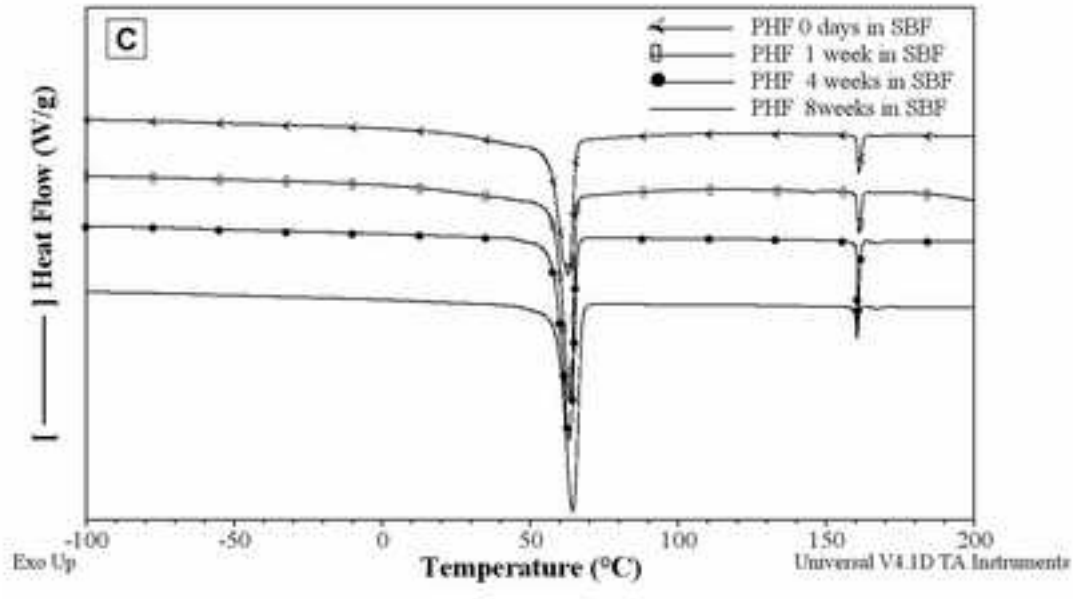

Figure 7D,E,F

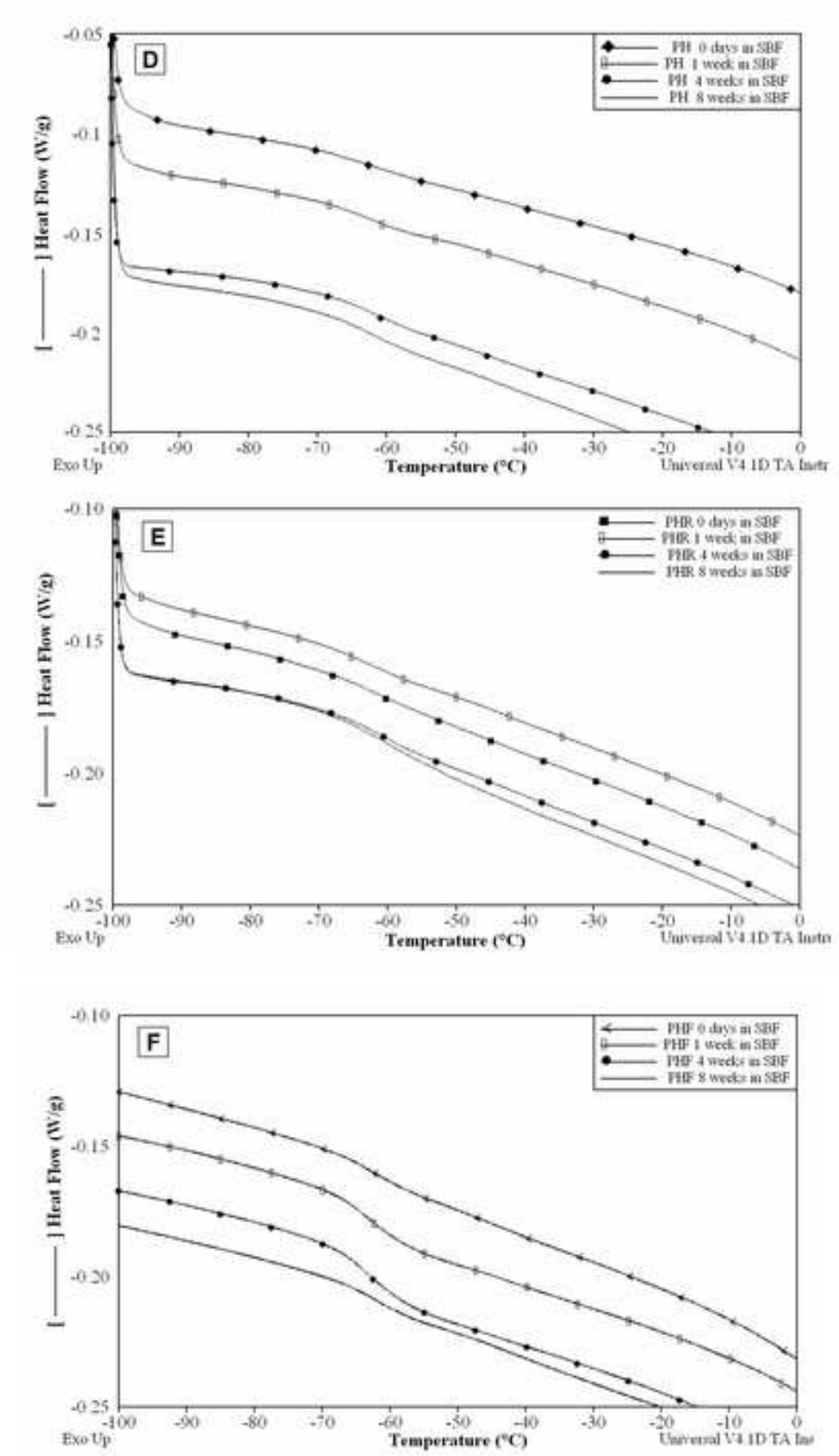

Figure 8